# A Novel Spatial-Temporal Adaptive Technique for Reconstruction of Dynamic MRI Series

Julia V Velikina[1] and Alexey A Samsonov[2]
[1]University of Wisconsin - Madison, Madison, Wisconsin, United States, [2]University of Wisconsin - Madison, WI, United States

**Introduction.** Clinical requirements on depiction of dynamic processes in the human body often impose data acquisition speed demands incompatible with standard MRI speed and SNR limits. Multiple reconstruction algorithms were proposed to provide useful images from significantly undersampled MRI data thereby providing higher time frame rates. One promising family of such techniques exploits spatio-temporal correlations in MR image series by assuming that temporal progression of each pixel can be represented as a linear combination of a few properly chosen temporal basis waveforms[1-3]. Performance of these techniques critically hinges on the choice of the temporal basis, which has to be large enough to represent the variety of temporal behaviors in the image series adequately. On the other hand, larger basis size leads to decreased acceleration capabilities and increased noise/aliasing artifacts. Basis is typically obtained by performing principal component analysis (PCA) on low-resolution training data. While PCA provides optimal representation of common mode behavior for a given basis size, representation of smaller temporally distinct features may require excessively large number of PCs. As a result, whole image PCA-based techniques may provide only a limited acceleration to applications with rich temporal dynamics, such as cardiac imaging or time-resolved angiography, or risk misrepresenting temporal behavior. In phase-contrast velocimetry, it was proposed[4] to subdivide the field-of-view (FOV) into three compartments according to velocity direction and choose a separate basis set for each of them. However, it is unclear if it is applicable to situations in which partitioning of pixels is not as straightforward or when deviating temporal behavior constitutes only a small part of the image. A different approach, MOCCO[5], avoids hard-constraining by temporal basis functions and allows deviations from common mode temporal behavior via robust $\ell_1$ norm, thus using fewer basis functions and simultaneously improving fidelity of the reconstruction. Still, for more complex temporal dynamics MOCCO-reconstructed images may suffer from residual bias due to inaccurate modeling of the image series by just a few globally learned PCs. In this work, we propose a novel reconstruction method, spatially adaptive MOCCO (MOCCO-SA), which iteratively partitions FOV into several clusters according to their temporal behavior and reconstructs each cluster using its own temporal basis whose modes and size are automatically adapted to capture localized temporal dynamics.

**Theory and Implementation.** The problem reconstructing image series $f$ is system of linear equations $\mathbf{E}f = \bar{\mathbf{b}}$, where $\mathbf{E}$ is encoding matrix, and $\bar{\mathbf{b}}$ is the vector of measured k-space data for all time frames. If k-space data is incomplete, the above equation has infinitely many solutions. To isolate a single solution, dimensionality reduction methods[1-3] constrain $f$ to a low-dimensional subspace $\boldsymbol{W}$ spanned by the chosen basis waveforms $(\boldsymbol{w_k})$. If $\boldsymbol{D}^*: w \to (< w, \boldsymbol{w_k} >)$ is the analysis operator for the system $(\boldsymbol{w_k})$ mapping each waveform into its coefficient sequence, and $\boldsymbol{D}$ is the synthesis operator mapping coefficients $(c_k)$ to a waveform $\sum c_k \boldsymbol{w_k} \in \boldsymbol{W}$, then $\boldsymbol{DD}^*$ is a linear projector onto $\boldsymbol{W}$. Thus, by searching for solution only within $\boldsymbol{W}$, $\ell_2$ methods[1-3] impose the requirement $\boldsymbol{DD}^* f = f$ on $f$. MOCCO relaxes this condition by allowing waveforms that are "close" to $\boldsymbol{W}$, i.e. requiring $\boldsymbol{DD}^* f \approx f$ for most pixels and solving $f = \arg\min_f \left( \|\boldsymbol{E}f - b\|_2^2 + \lambda \|(\boldsymbol{DD}^* - \boldsymbol{Id})f\|_{l_1/l_2} \right)$ (note that choosing large $\lambda$ and $\ell_2$ penalty effectively constrains $f$ to $\boldsymbol{W}$). MOCCO-SA allows for further temporal variability by making the action of operator $\boldsymbol{DD}^*$ dependent on pixel location. If $\boldsymbol{\Omega} = \{\Omega_1, \dots, \Omega_M\}$ is a partition of FOV and $(\boldsymbol{w_k^m})_{k=1}^{K_m}$ is a set of basis waveforms for pixels in $\Omega_m$, we define $\boldsymbol{D_\Omega D_\Omega^*} f(x,t) = \sum_{k=1}^{K_m} < f(x,\cdot), \boldsymbol{w_k^m} > \boldsymbol{w_k^m}(t)$ if $x \in \Omega_M$. MOCCO-SA alternates between estimating a partition $\boldsymbol{\Omega}$ according to typical temporal behaviors and estimating $f$ by solving $f = \arg\min_f \left( \|\boldsymbol{E}f - b\|_2^2 + \lambda \|(\boldsymbol{D_\Omega D_\Omega^*} - \boldsymbol{Id})f\|_{l_1/l_2} \right)$ as detailed in Fig. 1. Initial guess perform a global PCA of low resolution image estimate and thus is equivalent to regular MOCCO. Subsequent partitioning is performed using k-means clustering algorithm[6] with cosine-measured distance with 20 repetitions to avoid errors due to stochastic nature of the algorithm. Although the number of clusters can be determined automatically[6], in this work it was set to 4. Basis waveforms for each cluster were extracted from PCA corresponding to singular values whose relative rate of change stayed above the threshhold equal to mean singular value. With this criterion, the number of basis waveforms varied from 1 to 4. MOCCO minimization was implemented using iteratively reweighted least squares algorithm. The least squares step was performed using conjugate gradient algorithm with stopping criterion of relative error falling below 1e-8. The refinements of partitions were stopped when two subsecuent partitions were correlated above 0.95.

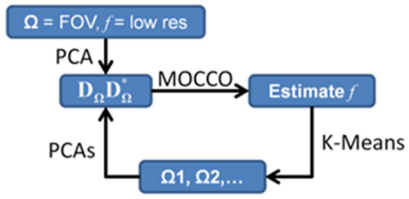


**Figure 1.** Diagram of the proposed method.

**Methods.** We performed initial evaluation of the proposed technique on numerical contrast-enhanced (CE) angiography phantom and in-vivo myocardial perfusion data. Undersampled data were reconstructed using regular and MOCCO-SA techniques (with three clustering itertions) with both $\ell_2$ and $\ell_1$ penalty terms. A 128x128x32 numerical phantom consists of a non-zero constant background with 9 circular objects representing vessels of different radii with gamma-variate waveforms shifted in time to simulate different contrast arrival times (Fig.2 a-b). White Gaussian noise (std=10% of max signal) was added to the phantom, and k-space data was computed simulating single coil variable density random sampling (net acceleration R=4). An 11x11 central square was sampled in all frames and used to produce the low resolution estimate. A fully sampled single coil 120x128x40 dynamic CE myocardial perfusion acquisition was retrospectively undersampled using variable density randomized phase encoding lines (net acceleration R=3) and 11 central lines sampled in all frames to obtain initial low resolution estimate.

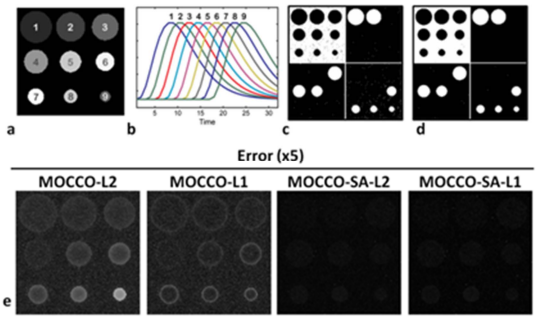


**Figure 2.** Simulation study: **a.** Phantom structure. **b.** Corresponding vessel time courses. **c,d.** Clustering after first and last iterations, respectively. **e.** Reconstruction errors averaged in time dimension for different techniques.

**Results.** As MOCCO-SA partitions the FOV into 4 clusters, initially misclassified background pixels (Fig. 2c) are correctly placed after the fourth iteration (Fig.2d), allowing for use of a single basis function for this cluster, which significantly reduced noise in MOCCO-SA recontructed images (Fig. 2f). Vessels were classified into three clusters according to similarity of their temporal behavior, allowing use of 2 PCs for cluster 2 and 3 PCs for clusters 3 and 4. Four PCs were used in regular MOCCO algorithms, resulting in residual artifacts due to insuffiecient approximation power (Fig. 2f). However, use of more PCs leads to prohibitively high noise amplification (not shown). Figure 3a displays a single frame with peak contrast in right ventricle, while images in Fig. 3b-d illustrate improvement of reconstruction error from regular MOCCO with $\ell_2$ (b) and $\ell_1$ (c) penalty terms to MOCCO-SA with $\ell_1$ penalty term (Fig.3d). Randomized phase encoding sampling is known to be less compatible with constrained reconstructions than 2D random sampling due to highly coherent aliasing artifacts (Fig.3b-c), which are reduced by MOCCO-SA (Fig.3d).

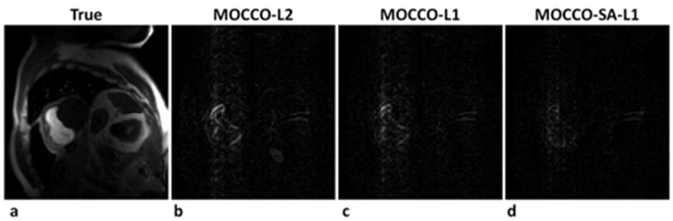


**Figure 3.** A single representative time frame of myocardial perfusion dataset. **a.** True image. **b-d.** Reconstruction errors (x3) for $\ell_2$ and $\ell_1$ MOCCO and MOCCO-SA with $\ell_1$.

**Discussion and Conclusions.** We presented a novel spatially adaptive reconstruction technique, which in initial studies provided noticeable improvement over corresponding techniques relying on temporal basis representation of the whole image series. The advantage of the proposed approach comes from its ability to use several temporal bases that are adapted both in modes and size to local temporal dynamics according to FOV partition. Such spatial adaptivity improves representation capabilities of local bases, thereby reducing their size and resulting in reduced noise and aliasing artifacts. Two potential advantages of this method over previously proposed compartment-based reconstruction techniques come from iterative refinement of FOV partitioning, which drastically reduces pixel misclassification, and from the use of robust $\ell_1$ norm, which safeguards against model inaccuracies. While the proposed technique was demonstrated with $\ell_1$ and $\ell_2$ MOCCO reconstruction (the latter equivalent to basic PC basis reconstruction), it can be used with other temporal basis reconstruction techniques.

**References:** 1. Liang ZP, Proc. ISBI 2007: 988-91. 2. Zhao B *et al.* IEEE Trans. Med. Imag. 31(2012): 1809-20. 3. Pedersen H *et al.* Magn. Res. Med. 62(2009):706-16. 4. Giese D *et al.* Magn. Res. Med. 69(2013):434-43. 5. Velikina JV *et al.* Proc. ISMRM 2012:13. 6. Forgy EW, Biometrics 21(1965):768-69.